Analysis of flocculation in a jet clarifier. Part 1 – Global and local hydrodynamic analysis

Ploypailin Romphophak, Claude Le Men, Arnaud Cockx, Carole Coufort-Saudejaud, Pisut Painmanakul, Alain Liné

Analysis of flocculation in a jet clarifier. Part 1 – Global and local hydrodynamic analysis

Ploypailin Romphophak[1,2], Claude Le Men[1], Arnaud Cockx[1], Carole Coufort-Saudejaud[3], Pisut Painmanakul[2], Alain Liné[1]

1: Toulouse Biotechnology Institute, Bio and Chemical Engineering (TBI), University of Toulouse, CNRS, INRA, INSA, Toulouse, France

2: Department of Environmental Engineering, Faculty of Engineering, Chulalongkorn University, Bangkok, Thailand

3: Laboratoire de Génie Chimique (LGC), Université de Toulouse, CNRS, INPT, UPS, Toulouse, France

Corresponding author: Alain Liné, alain.line@insa-toulouse.fr

Keywords

Jet clarifier, hydrodynamics, particle image velocimetry, velocity gradient

Abstract

Jet clarifier combines jet hydrodynamics, flocculation and settling in a unit operation. Generally, Camp and Stein *Gt* parameter is recommended to evaluate clarifier efficiency, where *G* stands for a global velocity gradient and *t* a characteristic time scale (contact time). In this work, a quasi-two-dimensional jet clarifier is developed to make easier the hydrodynamic analysis of the flocculation zone of a jet clarifier. Measurements of instantaneous velocity field are performed by means of particle image velocimetry (PIV). PIV data are processed to visualise the strong circulation induced by the jet in the flocculation zone. Characteristic time scales related to macromixing are then extracted. Based on PIV data processing, local and instantaneous shear rate are estimated. The analysis of space averaged velocity gradient *G* is presented. The range of *G* is 2 to 15 s^{-1} whereas the residence time decreases

from 4 to 1 hour. Based on the hydrodynamic analysis, the parameter *Gt* is shown to be constant around 30,000 for different jet flow rates. Efficiency of such jet clarifier can thus be foreseen.

1. Introduction

In general, the target of surface water treatment consists in removing suspended particles that cause turbidity in water. Jet clarifier is the one type of solid contact clarifier, coupling flocculation and clarification (sedimentation zone) in a single unit (Degremont, 2007; Pani and Patil, 2007; Romphophak et al., 2016). In many research, the performance of the flocculator reactors were measured by residual turbidity (Garland et al., 2017). Normally, the turbidity removal efficiency of the free jet flocculator is about 70 to 75% (Randive et al., 2018). Nonetheless, the performance of the jet clarifier which is investigated in this study is about 80%. This jet clarifier was designed based on the criteria such as residence time, sedimentation and surface loading rate. Afterward, the trial and error method was used to reach the appropriate operating conditions by varying the inlet flow rates, the height of the sludge blanket, the gap ratio between the sedimentation wall section and the flocculation, and the diameter of the cone base diameter of truncated of flocculation zone; some of the appropriate conditions of this reactor's geometry were presented in Romphophak et al., (2016),. Indeed, the scale of the jet clarifier presented in the previous paper is 4 times larger than the present scale, but the performance of the reactor in different scales is the same. However, the key phenomena that control the flocculation mechanisms are not clearly understood. Sobrinho et al. (1996) also mentioned that the effluent residual turbidity was essentially independent of the flow rate and associated this result to a nearly constant value of *Gt*. The possible reasons were proposed without any evidence or proof. For example, Gt may be constant because when the flow increases through the chamber reactor, the mixing intensity increases, and the retention time decreases. The higher mixing intensity (gradient velocity) may be balanced by the shorter retention time, resulting in a nearly constant GT value.

Furthermore, the authors based their analysis on head loss to estimate the velocity gradient. In the present study, the floc size distributions are independent of the flow rate too (see part 2 of this paper). The present analysis of the hydrodynamics of a jet clarifier is aimed at better understanding the physical phenomena explaining these independencies.

Commonly, the hydraulic flocculators have been designed based on a global parameter *G t* where *G* stands for the global velocity gradient and *t* stands for contact time (Camp & Stein, 1943; Pedochi & Piedra-Cueva, 2005; Garland et al., 2017; Marques and Ferreira, 2017). In flocculation, the Camp and Stein criteria *G t* recommended to achieve efficient flocculation is usually in the following range:

$$10^4 < G\ t < 10^5 \quad (1)$$

The analysis of *G t* in clear water and in the flocculation zone of a jet clarifier will constitute the final outcome of this paper; the global criteria *G t* will be highlighted by a local analysis of *G t*, where *G* will be the local shear rate and *t* is a hydrodynamic characteristic time.

Modelling of aggregation and break-up of flocs is out of the scope of this paper. However, it is important to recall how flocculation is related to hydrodynamics. One of the first attempts to quantify the collision rate of particles induced by hydrodynamics was proposed by Smoluchowski (1917) in terms of local velocity gradient. Then, Camp and Stein (1943) extended Smoluchowski's model of velocity gradient *G.* They also introduced a global parameter, the root mean square velocity gradient G_{RMS}, in terms of power input by unit mass of liquid (W/kg). As reported by Pedocchi and Piedra-Cueva (2005), "the denomination velocity gradient has created some confusion about the physical interpretation of this parameter". Indeed, the work of Camp and Stein has been revisited by many workers (among them Cleasby, 1984; Clark, 1985; Kramer and Clark, 1997). It is now accepted that the velocity gradient is defined as the square root of the viscous dissipation rate of kinetic energy (W/kg) divided by the kinematic viscosity. It is thus identical to the local shear rate and is defined as:

$$G = \dot{\gamma} = \sqrt{\frac{1}{2} tr\left(\overline{S^2}\right)} = \sqrt{\frac{1}{2} tr(\bar{S}^2) + \frac{1}{2} tr(\overline{s'^2})} \quad (2)$$

Where S is the symmetric part of the velocity gradient tensor. Here, $tr(\overline{S^2})$ is an invariant. The first term on the r.h.s. is related to the square of mean velocity gradients whereas the second one stands for the average of the square of the fluctuating (turbulent) velocity gradients. These two terms are respectively related to the viscous dissipation of the mean flow kinetic energy and to the viscous dissipation of the turbulent kinetic energy. In turbulent flow, the first one is negligible compared to the viscous dissipation of the turbulent kinetic energy. Averaged over the whole tank or clarifier, the dissipated power is equal to the power input.

The present study focuses on hydrodynamics, in terms of local and instantaneous velocity field, induced by the jet in the flocculation zone of a jet clarifier. The two key words being “jet” and “clarifier”, the bibliography analysis will consider these two terms. However, in terms of application in chemical engineering and water treatment, the flocculation-clarifier issue will be predominant.

1.1 Jet flow

Jets are used in many industrial or environmental applications. In the past, jet flow hydrodynamics was addressed theoretically, experimentally and numerically. Schlichting (1933) was the pioneer to study jets. Bickley (1937) derived analytical solutions of jet flows; he demonstrated that the developing jet flow entrains external fluid, increasing the flow rate and decreasing the axial velocity, thus preserving constant momentum. Based on experiments, Miller & Comings (1957) showed that the jet decreases axially as the square root of the axial position along the jet (the origin being at the orifice outlet) and the jet size enlargement was shown to increase linearly with the axial position. These hydrodynamic phenomena will be investigated in our jet clarifier.

A jet is usually characterized by the Reynolds number at the injection. The Reynolds number is classically defined as:

$$Re = \frac{\langle U \rangle \, d}{\nu} \tag{3}$$

Where $\langle U \rangle$ is the cross-averaged discharge velocity from the nozzle (m/s), *d* is the circular orifice nozzle internal diameter (m) and ν is the kinematic viscosity of the fluid (m²/s). Referring to Pearce (1966) conclusion, there is no turbulence below 500 and fully turbulent jet starts at 3000. Since in our study, the Reynolds number vary between 1000 and 4000, it corresponds to the transition from laminar to turbulent jet flow. Both jet structure and stability aspects of transition flows have also been reviewed by Mollendorf & Gebhart (1973). A submerged liquid jet from a circular orifice nozzle into a similar liquid exhibits three characteristics regions: (1) a developing flow region: about 10 nozzle diameters long; this region is called potential conic region; (2) a developed flow region: up to 100 nozzle diameters from the orifice; (3) a terminal region: above 100 nozzle diameters from the orifice.

It was reported that instabilities appear in the sheared layers induced by the submerged liquid jet. Downstream, mixing is controlled by the entrainment of surrounding liquid in the decelerating jet velocity region. In the developed flow region, the jet structure weakly depends on inlet conditions, in particular on discharge velocity profile. In our study, the discharge flow corresponds to laminar to turbulent flow pattern in the circular nozzle. In the developed flow region, the liquid flow induced by the jet exhibits radial enlargement. This was first addressed by Lee & Chu (1996), who assumed that the jet radial size increase was proportional to the discharge jet velocity. This gradual enlargement is related to a decrease of the mean velocity in the jet and to the entrainment of external fluid; thus, the analysis of the axial evolution of the jet radial size will be investigated.

1.2 Clarifier

The first issue of clarification is related to flocculation. Indeed, flocculation efficiency is related to mixing in the jet clarifier. The bibliographic analysis must thus focus on mixing induced by jets, in different geometries. In terms of mixing, Fossett and Prosser (1949) and Fossett (1951) reported inclined side-entry jet mixing of free turbulent jets in cylindrical tanks. Fox and Gex (1956) investigated both laminar and turbulent inclined side-entry jet regimes and concluded that the main phenomena controlling the mixing time was the momentum source injected by the jet in the tank. In terms of

vertical jet mixer, studies were reported by Hiby and Modigell (1978) and by Lane and Rice (1981, 1982) in a hemi-spherical base, reporting shorter mixing times compared to flat base cylindrical tank. Maruyama, Ban, and Mizushina (1982) found that the mixing time in jet flow tank depended on the liquid depth, nozzle height, and nozzle angle, and the mixing time is a consequence of jet axis length. Maruyama, Kamishima and Mizushina (1984) reviewed mixing induced in different geometries using horizontal, inclined and vertical jets. However, although global circulation was presented and global mixing time were determined, there was neither data nor information on the local phenomena controlling mixing.

Grenville and Tilton (1996) studied the free jet mixing time of the tank with $H/D \leq 1$ where H is the fluid depth and D is the vessel diameter. They proposed that the mixing time had been correlated by turbulent kinetic energy dissipation rate (or power per unit mass). The turbulent kinetic energy dissipation rate at the end of the jet's free path can be used to estimate the mixing rate and it controlled the mixing rate for the whole vessel. Then, Grenville and Tilton (1997) proffered the correlation based on the jet nozzle angle and compared their model with the circulation time model. They found that both models can be used to predict accurate mixing time in the tank and their previous model presented in 1996. Further, Grenville and Tilton (2010) continued their work by studying the mixing time in various tank geometries and found that their jet turbulence model fitted in the range of $0.2 < H/D < 3$ and the ratio of mixing time to circulation time is not constant but rather depending on the ratio of fluid depth to diameter of the vessel.

Jayanti (2001) reported that the position of the "eye" of the circulation pattern induced by a jet is a key parameter for mixing and it depends on the tank geometry. Jayanti compared hemi-spherical base, ellipsoidal base, conical base with a half cone angle of 31° and conical base with a half cone angle of 58°. The best shape was found to be conical base with a half cone angle of 31°. In this case, the "eye" of the recirculation pattern is half the overall height, the recirculation is quite strong and there is no low velocity region. This conclusion probably contributes to explain the efficiency of the present jet

clarifier since flocculation zone corresponds to a divergent (2D cone). Wasewar (2006) investigated design of jet mixing tank. His review summarizes different studies of jet mixed tank parameters (tank geometry, jet configuration, jet velocity, jet diameter, jet flow rate and fluid properties) to get an optimum design. He pointed out that mixing time is an important parameter to design jet tank devices.

Perumal and Saravanan (2012) and Randive et al. (2018) investigated jet mixing; they pointed out that the difference between jet and bulk liquid velocity creates a turbulent mixing zone along the jet boundary. In this mixing zone, some part of the surrounding fluid is circulated at high velocity and create a circulation loop, thus leading to mix the bulk of the liquid. This kind of circulation loop induced by the jet will be investigated in this paper. Randive et al. (2018) reviewed the jet mixing in the flocculation process and summarized several models to estimate the mixing time in terms of other parameters such as jet velocity, jet diameter, jet path length, and tank diameter and height.

Kennedy et al. (2017) studied the effect of the distance between injection and suction ports on the control mixing time of submerged recirculation jets. They found that the distance between the ports can be used to control mixing time at the same value of injection velocity and an empirical correlation to predict the mixing time under short-circuiting conditions of the flow is dominant, which retains the same dependence of mixing time on the injection velocity and the tank diameter.

Garland et al. (2017) analysed the effects of Gt on turbidity removal by hydraulic flocculator, indicating better performance when a floc blanket had been formed. They concluded that appropriate mixing time is a factor that can be used to limit the size of the clarifier. In our paper, since only clear water hydrodynamics is investigated, floc blanket will not be accounted for.

In order to investigate the hydrodynamics of the new jet clarifier, PIV experiments will be presented and discussed, both in terms of jet characteristics and in terms of flow structure leading to the estimation of Gt criteria.

2. Material and methods

2.1 Set up

The laboratory pilot was designed to investigate local hydrodynamic of the jet clarifier. A pseudo-two-dimensional jet clarifier was designed with 56 cm. high, 95 cm. long, and 10 cm. thickness, which is named as a flat quasi-bidimensionnal (Q2D) clarifier. The Q2D jet clarifier was constructed using Plexiglass (PMMA) (1 cm thick) enabling velocity measurement with especially the flocculation zone, a cone-shape, inside the reactor. The liquid volume in the pilot is 42 litres. Figure 1 illustrates the pilot; the inlet flow was regulated and measured by a micro gear pump (WT3000-1JA, Longer Precision Pump Co.). The jet flow is discharged by a nozzle of 4 mm diameter. The water flows outside the Q2D jet clarifier over weirs (outlet) and a symmetrical flow is induced if we pay attention to the equal repartition of the two outflows.

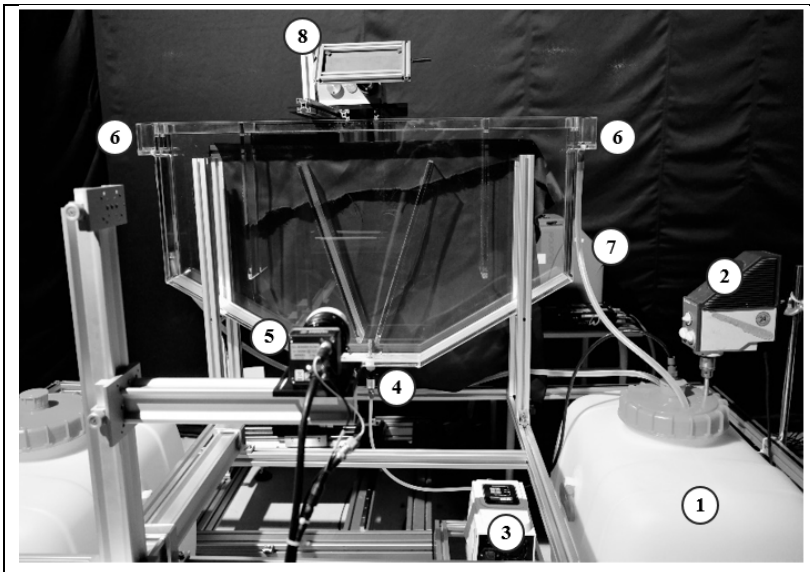

1. Water preparation tank
2. Agitator with motor
3. Micro gear pump
4. Inlet and jet nozzle
5. CCD camera
6. Outlet
7. Laser generator
8. Light source

Figure 1. Q2D jet clarifier experimental setup

The jet clarifier is made of two main zones: a flocculation one (mainly downstream the jet inlet 4, within the vertical divergent) and a settling one (downflow & upflow towards the outlet 6). The two zone are separated by inclined baffles with an angle of 40°. The liquid enters in the pilot by the nozzle

(4), then it flows upward to the free surface, leaves the flocculation zone by flowing over the two inclines baffles. The liquid flow is then downward (settling zone), between each inclines baffle and lateral vertical baffles. The liquid leaves the settling zone by flowing under the lateral vertical baffles. The liquid flows upward to the outlets (6).

As we will see, there is a strong recirculation induced by the jet in the divergent, creating long residence and efficient mixing. In this paper, we will focus on the hydrodynamics in the flocculation zone (mainly fields 1 and 2 of figure 2, and partially field 3).

2.2 PIV technique

The PIV system used in this study is the commercial system from Dantec Dynamics Co. (Denmark). The required basic elements include a double-pulsed Nd: YAG laser (big sky laser of 30 mJ.) operated at a trigger rate close to 10 Hz. Each pulsation was controlled by the trigger rate between 3 – 20 ms depending on the flow velocity. A CCD camera (Flow sense EO, Dantec Dynamic) was used to record the flow at each flash laser. The resolution of each recorded field is 200×200 mm^2 with a scale close to 0.1 mm/pixels (2048×2048 pixels^2). In this work, the Rhodamine B suspensions are well mixed in the water preparation tank by an agitator with the motor before feeding into the flat jet clarifier. The seeding particles are covered with the fluorescent dye Rhodamine B, for which maximum light absorption takes place at 532 nm, while the emission is in the red range with a maximum around 590nm. Hence, a laser light sheet in the green range (537nm) was used and a high pass light filter (> 570nm) was added to the camera. Thus, any light disturbances may be reduced as far as possible.

This technique enables acquisition of an instantaneous two-dimensional velocity field in a vertical plane. The vertical plane investigated in this study was fixed in the plane of symmetry of the pilot (at a position Z = 5 cm, half the depth of the quasi-2D pilot). For the jet clarifier, the hydrodynamics were studied in four fields to measure the velocity field in the whole flocculation zone, illustrated in Figure 2, but in this paper, the hydrodynamic study focuses on these fields corresponding to the jet mixing flocculation zone.

The size of each PIV image was fixed to 200 mm. Each velocity field, measured over a square 200 x 200 mm², is composed of the two components (U horizontal and V vertical) of the instantaneous velocity on a 127 x 127 squared matrix. Thus, the distance between two vectors (so called PIV filter) is 1.57 mm (16 pixels).

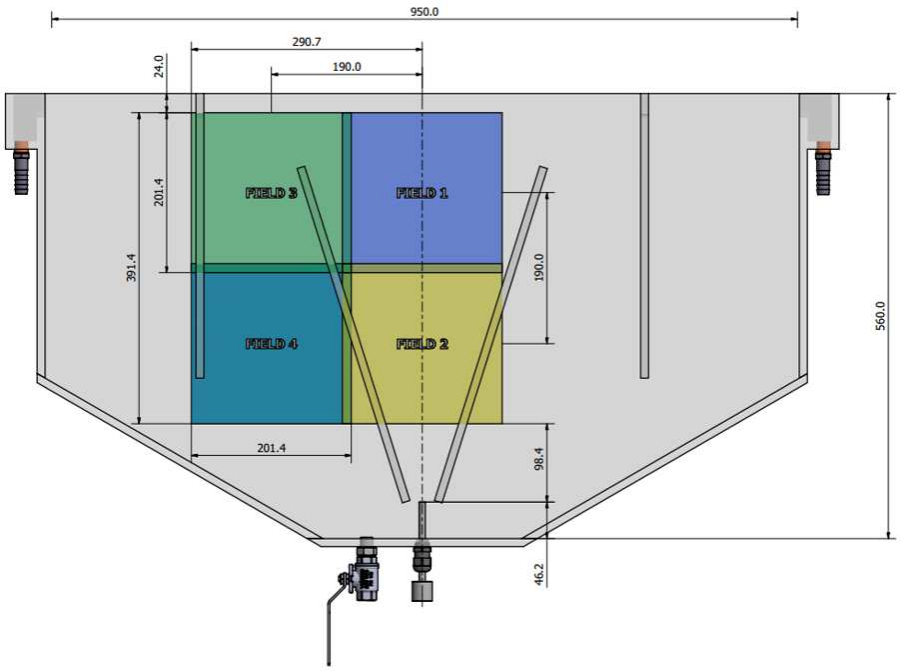

Figure 2. PIV windows in the vertical plane of symmetry of the jet clarifier (lengths are expressed in mm)

2.3 PIV postprocessing

In order to check statistical convergence of the data, the cumulative mean average of U and V mean velocity components as well as u'^2 and v'^2 variances are plotted on figure 3 (a & b). The ordinate represent the mean values averaged over a number of events (instantaneous measurements) given in abscissa.

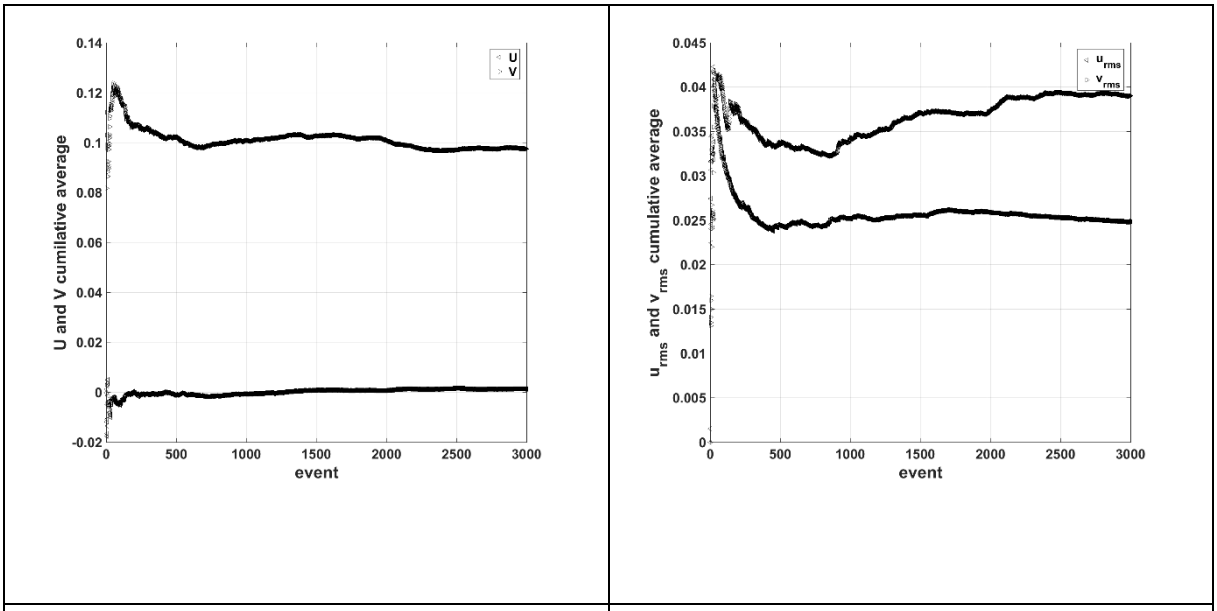

(a) mean velocity components | (b) variance fluctuating velocity components

Figure 3. Cumulative averaged of (a) mean velocity components and (b) variance of fluctuating velocity components at 49 L/h in the centre of field 2

Figure 3 shows that 3000 instantaneous velocity field are sufficient to derive statistically converged mean and rms velocity components.

2.4 Global analysis

Before performing local analysis of the hydrodynamic based on PIV, it is necessary to investigate global parameters. Three flow rates were investigated in our study. They are given Table 1, as well as the Reynolds number at the outlet of the orifice nozzle. The flow pattern in the 4 mm internal diameter circular orifice nozzle is laminar for the two lower flow rates and slightly turbulent for the larger one. Considering the downstream liquid jet, based on the Reynolds number at the outlet of the injection tube, and referring to Pearce (1966) the flow pattern of the liquid jet is laminar for Re smaller than 500 and fully turbulent for Re larger than 3000.

Two characteristic inlet parameters can be quantified. The flux of momentum at the injection is defined as:

$$J_0 = \iint \rho\, U(r)^2\, r\, dr\, d\theta = \rho\, S_{CS}\, \langle U^2 \rangle = \rho\, S_{CS}\, C_2\, \langle U \rangle^2 \quad (4)$$

Where S_{CS} is the cross-section of the circular orifice nozzle. Since the discharge velocity profile is not uniform, C_2 has been introduced to relate the average of the square of the velocity $\langle U^2 \rangle$ to the square of the mean discharge velocity $\langle U \rangle$.

The supplied power can be derived from the flux of kinetic energy at the injection:

$$P = \iint \frac{1}{2}\, \rho\, U(r)^3\, r\, dr\, d\theta = \frac{1}{2}\, \rho\, S_{CS}\, \langle U^3 \rangle = \frac{1}{2}\, \rho\, S_{CS}\, C_3\, \langle \bar{U} \rangle^3 \quad (5)$$

Here again, C_3 has been introduced to relate the average of the cubic of the velocity $\langle U^3 \rangle$ to the cubic of the mean discharge velocity $\langle U \rangle$.

Assuming laminar flow in the injection tube, one can express the radial discharge velocity profile in terms of parabolic profile:

$$\frac{U(r)}{U_{max}} = 1 - \left(\frac{r}{R}\right)^2 \quad (6)$$

Where the maximum velocity is twice the mean discharge velocity $\langle U \rangle$. One can thus easily derive analytically the two coefficients C_2 and C_3 in laminar flow as:

$$C_2 = \frac{\langle U^2 \rangle}{\langle U \rangle^2} = \frac{4}{3} \qquad C_3 = \frac{\langle U^3 \rangle}{\langle U \rangle^3} = 2 \quad (7)$$

In turbulent flow, a power law velocity profile is assumed:

$$\frac{\bar{U}(r)}{\overline{U_{max}}} = \left(1 - \frac{r}{R}\right)^{\frac{1}{6}} \quad (8)$$

Where the power 1/6 depends on the Reynolds number (*Re* close to 4300 in this work), following Schlichting book.

One can thus easily derive analytically the two coefficients C_2 and C_3 in turbulent flow as:

$$C_2 = \frac{\langle U^2 \rangle}{\langle U \rangle^2} = 1.03 \qquad C_3 = \frac{\langle U^3 \rangle}{\langle U \rangle^3} = 1.077 \quad (9)$$

The numerical values of C_2 and C_3 are reported in Table 1 for the 3 flow rates. The averaged dissipated power per unit mass is defined as:

$$\langle \epsilon \rangle = \frac{P}{m} = \frac{1}{2} \frac{S_{CS}}{Vol} C_3 \langle \overline{U} \rangle^3 \quad (10)$$

Where *m* is the mass of liquid (kg) in the pilot and *Vol* is the volume of water in the pilot (*Vol = 42 L*).

One can finally derive the volume averaged velocity gradient G or volume averaged shear rate:

$$G = \sqrt{\frac{\langle \epsilon \rangle}{\nu}} \quad (11)$$

The residence time in the whole clarifier is simply given by the volume of liquid in the pilot divided by the discharge flow rate Q.

$$t = \frac{Vol}{Q} \quad (12)$$

From the velocity gradient *G* and the residence time *t*, one can estimate the Camp and Stein parameter:

$$G\ t = \sqrt{\frac{V}{2\ S_{CS}\ d}\ C_3}\ \sqrt{Re} \quad (13)$$

Where, as previously, $\sqrt{\frac{2\ V}{S_{CS}\ d}\ C_3}$ ranges between 1850 and 1350. *G t* is thus between 25,000 and 45,000; recall that in flocculation, *G t* is usually in the following range $10^4 < G\ t < 10^5$(eq. 1).

Table 1. Global hydrodynamic characteristics for the 3 flow rates

Q Flow rate (L/h)	11	19	49
U injection (m/s)	0.24	0.42	1.08
Re tube	970	1680	4330
$C_3 = \langle U^3 \rangle / \langle U \rangle^3$	2	2	1,077
Supplied power (mW)	0.36	1.86	17.2
$\langle \epsilon \rangle$ (W/kg)	4.3 e-6	2.2 e-5	2 e-4

$\langle G \rangle$ (s^{-1})	2.1	4.7	14.3
J_0 (kg m/s²)	0.001	0.004	0.020
Residence time (h)	3.82	2.21	0.86
G t	28,500	37,500	44,150

3. PIV results in the flocculation zone

Results concern the hydrodynamics of the flocculation zone (estimated to 7 litres volume), located in the vertical divergent of the jet clarifier (figure 1). In this section, results are organised as follows: velocity fields in zones 1 and 2 of the pilot (figure 2) are plotted, exhibiting a large circulation. Circulation flow rates are estimated as well as circulation time that are compared to residence time in this zone. The characteristic shape of the jet is also investigated, in terms of vertical distribution of its width. Then the outflow is analysed, and the outward flow rate is shown to be close to the inlet flow rate.

Mean velocity fields are plotted on figure 4 for the 3 flow rates and the 2 measurement fields 1 and 2; only the left-hand side of the PIV fields is plotted. These velocity fields exhibit similar circulation loops generated by the vertical jets. The eyes of circulations are located at Y = 340, 360 and 380 mm for the respective flow rates 11, 19 and 49 LPH. The differences between the 3 flow fields seem thus to be weak.

Each horizontal profile of vertical mean velocity is processed. The vertical velocity is positive in the jet plume (upward flow) and negative outside (downward flow). The width of the jet can thus be estimated at each vertical position Y. In order to quantify the similarity of these flow patterns, the vertical profiles of plume width are plotted on figure 5(a). A gradual enlargement is observed and can be related to a decrease of the mean velocity in the jet and to the entrainment of external fluid. The evolutions of the jet plume widths for the 3 flow rates are very similar. As reported by Lee and Chu (1996), the jet plume width increases with increasing distance from the nozzle (located at Y = 0). The

estimation of the width increase with the distance is around 60 mm for 300 mm from the jet, it gives an angle for the jet development close to 10 degrees, much smaller than the geometrical angle between the two internal baffles.

The 3 eyes of circulations being located roughly in the same zones (- 80 < X < - 60 mm and 340 < Y < 380 mm), the horizontal profiles of vertical mean velocity at the location of the eye of circulation have been plotted on figure 5(b). The vertical velocity profiles are normalised by their maximum velocity, the three profiles can thus be superimposed.

From figure 5(b), it is possible to estimate the vertical flow rate, which will be considered as circulating flow rate Q_c, by integrating the horizontal profile vertical velocity between the axis of the pilot and the lateral position of the circulation eye. The width of the half jet plume being close to 50 mm, the thickness of the pilot being 100 mm, an axisymmetric jet could be assumed. Thus, 3 flow rates Q_c, called circulation flow rates have been determined. The values of the circulation flow rates Q_c are reported in table 2. They range between 12 and 15 times the inlet flow rates, indicating a huge entrainment and a strong recirculation in the flocculation zone.

Clearly, the structure of the flow slightly depends on the injected flow rate, indicating that the circulation loops are similar for the three injected flow rates.

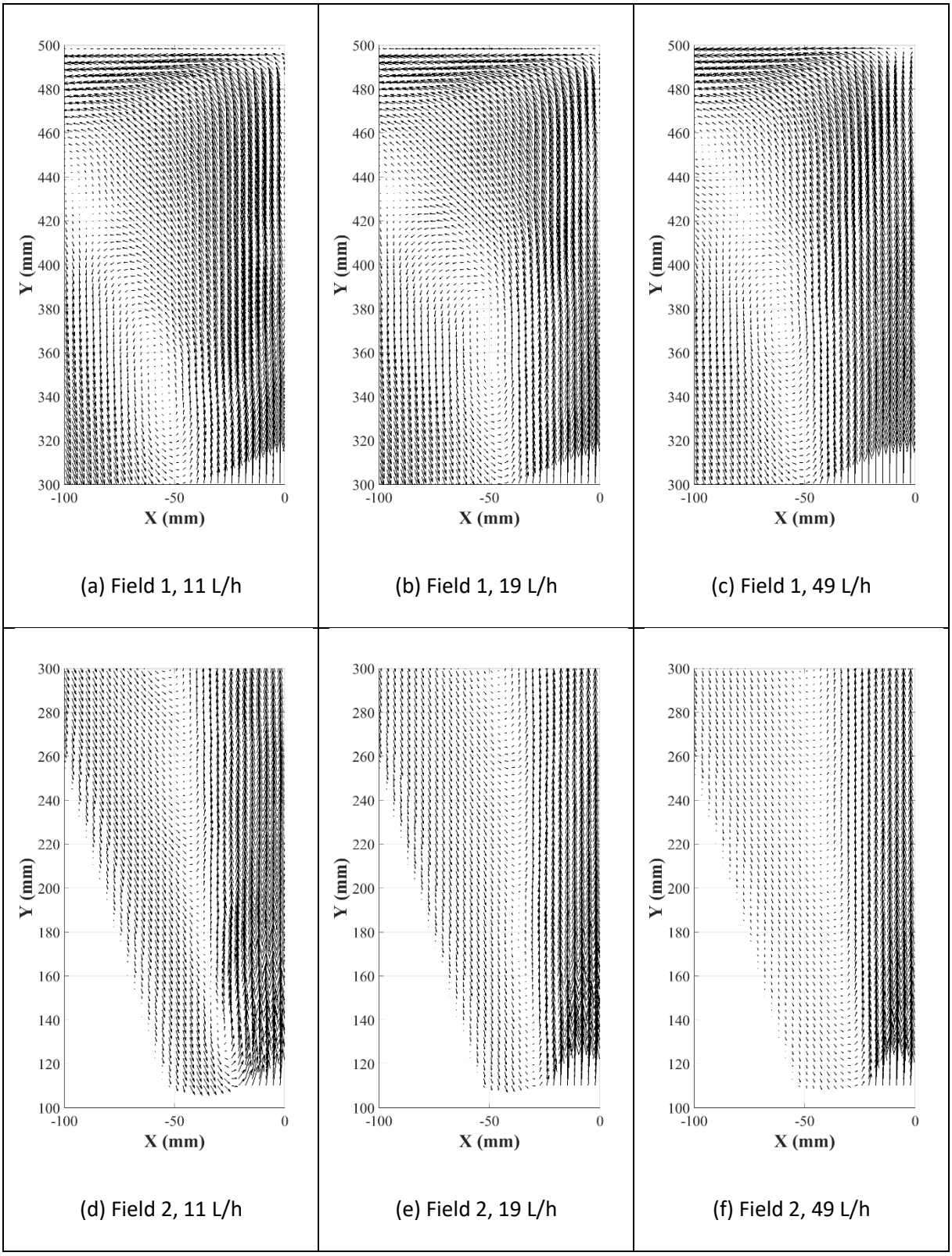

Figure 4. Mean velocity field for each injected flow rate

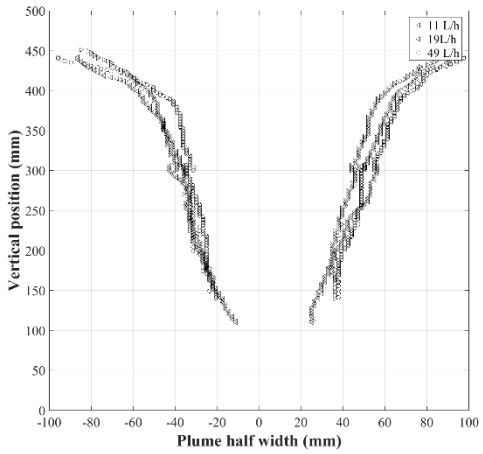

a- jet plume width

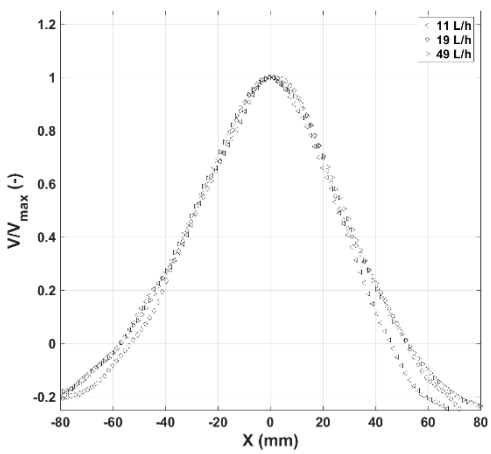

b- Axial mean velocity profile, at the location of the eye of recirculation

Figure 5. Jet flow characteristics: (a) vertical distribution of the width of the jet plume and (b) horizontal profile of axial velocity (for the three flow rates: < 11L/h, o 19 L/h, > 49 L/h)

The residence time in the flocculation zone (inside the vertical divergent) is estimated as the ratio of volume of this zone (estimated to 7 liters) divided by the injected flow rate Q. The residence times are thus equal to 38.2, 22.1 and 8.6 minutes. Given the circulation flow rates Q_c, the circulation time can be estimated as the ratio of volume of the flocculation zone (estimated to 7 liters) divided by the circulation flow rate Q_c. Clearly, the circulation times are very small compared to the residence time of the flocculation zone. Consequently, the fluid particles will travel along circulation loops at least 10 times before flowing outward the flocculation zone. This constitutes an efficient macro-mixing zone.

Table 2. Processed hydrodynamic characteristics for the 3 flow rates

Q (L/h)	Injected flow rate	11	19	49
U (m/s)	Injection velocity	0.24	0.42	1.08
t_{RF} (min)	Residence time in flocculation zone	38.16	22.08	8.58

Q_c (L/h)	circulation flow rate	165	228	637
Q_c/Q	Ratio of circulation flow rate/and injected flow rate	15	12	13
t_c (min)	Circulation time	2.55	1.83	0.67

It is however important to evaluate the flow rate outside the flocculation zone. The velocity fields above the left inclined wall are plotted on figure 6 (a) to (c). Vertical profiles of horizontal velocities normalized by the velocity scale (derived as the ratio of the injected flow rate and the section above the wall 65x100 mm²) are plotted on figure 6 (d) for the three flow rates. Here again, flow field are similar for the 3 jet flow rates.

From figure 6 (d), it is possible to calculate the net flow rate per depth length by integrating the velocity profile above the internal wall. The results are given in Table 3. The positive (outward), negative (inward) and total flow rates per unit depth length are estimated. A Reynolds number can be derived based on the average velocity (U_{total}) and the hydraulic diameter of the rectangular cross-section (height 65 mm, depth 100 mm, hydraulic diameter close to 80 mm). The Reynolds numbers ranging between 100 and 150, the flow rate (in cubic meter per second) can be obtained by assuming laminar flow in this region. Since there are two outlets, one on the right side and another one on the left side of the flocculation zone, these estimated outward flow rates are compared to half the inlet flow rate. This ratio varies between 1 and 2.5. Consequently, one can conclude that the flow rate outside the flocculation zone is close to the injected flow rate, and much smaller than the circulation flow rate inside the flocculation zone (12 to 15 times the inlet flow rate). Consequently, there is a strong internal circulation in the flocculation zone (inside internal walls) but there is almost no circulation around the internal walls. Moreover, the negative flow rate directed inside the flocculation zone increases from 20% to 65% of the positive flow rate and then balances better. It means that the external flow around

the inclined baffle is proportionally reduced as confirmed by the decreasing of the ratio between the flow rate above the wall and the inlet flow rate from 2.5 to 1.

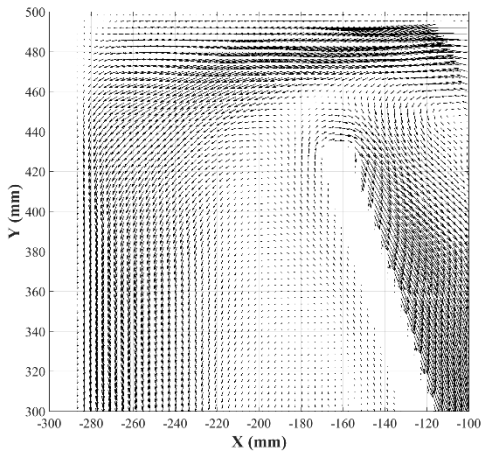

(a) Velocity field 11 L/h

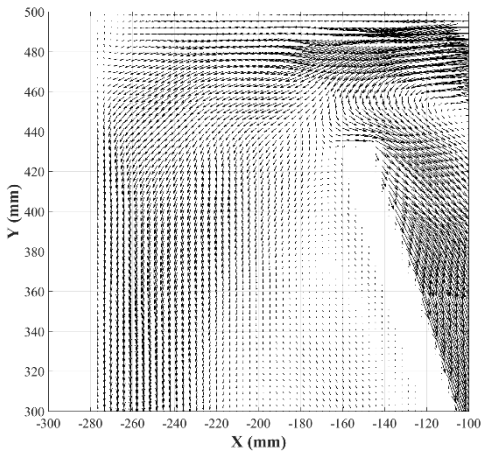

(b) Velocity field 19 L/h

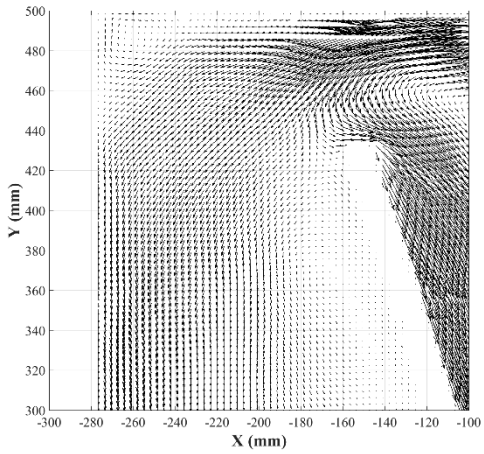

(c) Velocity field 49 L/h

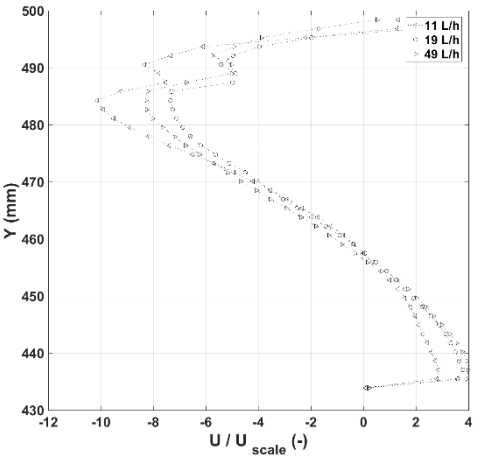

(d) Vertical profile of horizontal and normalized velocity above the internal wall

Figure 6 Characteristic flow above the internal wall bounding the flocculation zone.

Table 3. Characteristic data for the flow outside the flocculation zone

Q (L/h)	Injected flow rate	11 L/h	19 L/h	49 L/h
Q (m^3/s)	Injected flow rate	$3.05\ 10^{-6}$	$5.28\ 10^{-6}$	$1.3\ 10^{-5}$
Q_{total}($m^3/s/m$)	Total flow rate above the wall per width of pilot	$8.1\ 10^{-5}$	$9\ 10^{-5}$	$1.22\ 10^{-4}$
$Q_{outside}$ ($m^3/s/m$)	Positive flow rate, directed outside the flocculation zone	$1.\ 10^{-4}$	$1.34\ 10^{-4}$	$3.46\ 10^{-4}$
Q_{inside} ($m^3/s/m$)	Negative flow rate, directed inside the flocculation zone	$-1.9\ 10^{-5}$	$-4.22\ 10^{-5}$	$-2.25\ 10^{-4}$
U_{total} (m/s)	Total velocity	0.0013	0.0014	0.0019
$U_{outside}$ (m/s)	Positive velocity	0.0025	0.0035	0.0105
U_{inside} (m/s)	Negative velocity	-0.0008	-0.0016	-0.0071
Re	Re	104	112	152
$Q_{total\text{-}laminar}$ (m^3/s)	Total flow rate above the wall assuming laminar velocity profile along Z	$4.05\ 10^{-6}$	$4.5\ 10^{-6}$	$6.1\ 10^{-6}$
$Q_{total\text{-}laminar}$ / (Q /2)	Ratio of total flow rate above the wall and half the injected flow rate	2.6	1.7	0.95

In conclusion, the jet induces a strong circulation loop inside the flocculation zone (vertical divergent). Whatever the flowrate, 30 cm above the nozzle the angle of the jet development is close to 10°. The presence of the 2 inclined baffles (37°) has clearly an influence on the development of the jet since the circulation patterns are similar for the three flow rates. Characteristic time scales of the circulation have been estimated in Table 2. One can now investigate the distributions of velocity gradients.

4. Discussion on hydrodynamics for flocculation

In the section, both local-instantaneous and global (time and space averaged) velocity gradient are addressed.

On figure 7, the vertical profiles of four characteristic variables are plotted: the local mean vertical velocity, the viscous dissipation rate of kinetic energy, the Kolmogorov scale and the velocity gradient (shear rate). Figure 7(a) corresponds to the vertical profile of mean velocity along the axis (X=0), normalised by the inlet velocity. Clearly the profiles are identical, except in the lower zone, closer to the injection nozzle where the circulation around the internal baffle should modify the total flow rate that enter in the flocculation zone. This plot confirms that the global hydrodynamics induced by the jet is similar for the three flow rates and the vertical mean velocity is simply proportional to the injected flow rate.

From the instantaneous velocity fields, it is possible to estimate the local viscous dissipation rate of the mean flow kinetic energy and the local viscous dissipation rate of the turbulent kinetic energy. These dissipation rates are based on the 2D velocity measurement. Thus, they are estimated following the expressions:

$$\epsilon_{mean\ flow} = \nu \left[2 \left(\frac{\partial \overline{U}}{\partial x}\right)^2 + \left(\frac{\partial \overline{U}}{\partial y}\right)^2 + \left(\frac{\partial \overline{V}}{\partial x}\right)^2 + 2 \left(\frac{\partial \overline{V}}{\partial y}\right)^2 + 2 \left(\frac{\partial \overline{W}}{\partial z}\right)^2 + 2 \frac{\partial \overline{U}}{\partial y} \frac{\partial \overline{V}}{\partial x} \right] \quad (14)$$

$$\epsilon_{turbulent\ flow} = \nu \left[2 \overline{\left(\frac{\partial u\prime}{\partial x}\right)^2} + \overline{\left(\frac{\partial u\prime}{\partial y}\right)^2} + \overline{\left(\frac{\partial v\prime}{\partial x}\right)^2} + 2 \overline{\left(\frac{\partial v\prime}{\partial y}\right)^2} + 2 \overline{\left(\frac{\partial w\prime}{\partial z}\right)^2} + 2 \overline{\frac{\partial u\prime}{\partial y} \frac{\partial v\prime}{\partial x}} \right] \quad (15)$$

Figure 7(b) presents the vertical profiles of the horizontal averaged (along the width of the divergent) value of the viscous dissipation rate of total (mean flow + turbulent flow) kinetic energy. Figure 7(c) presents the vertical profile of the horizontal averaged (along the width of the divergent) value of Kolmogorov scale (η), based on the local viscous dissipation rate of the turbulent kinetic energy. These length scales range between 0.2 and 1 mm and are thus close to the PIV filter (validating the data

processing, Delafosse et al, 2011). Finally, the velocity gradient is estimated, based on equation (2). Here again, its average value along the width of the divergent is derived. In order to present non-dimensional velocity gradient, the horizontally averaged velocity gradient is multiplied by the depth of the pilot (h = 100 mm) and divided by the inlet velocity. The choice of inlet velocity as velocity scale is straightforward, but the choice of pilot depth (100 mm) as length scale is arbitrary. It leads to non-dimensional velocity gradients close to unity. Distinctly, the three curves of such normalised velocity gradients are identical, indicating that the velocity gradient is proportional to the inlet velocity.

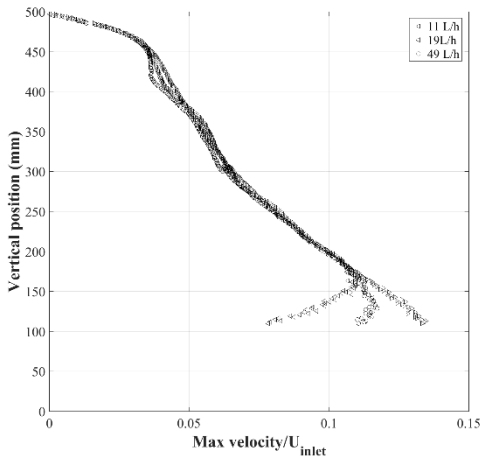

(a) normalized mean velocity components

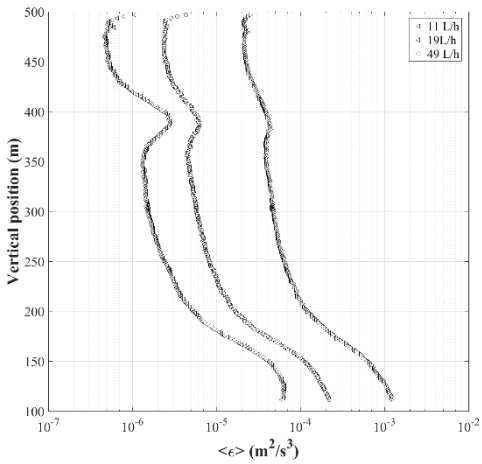

(b) horizontal averaged viscous dissipation rates of mean and turbulent kinetic energy

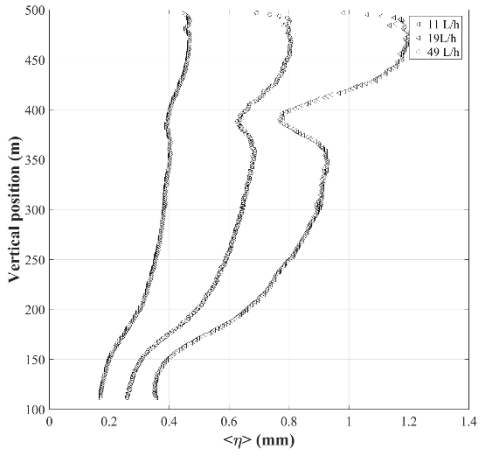

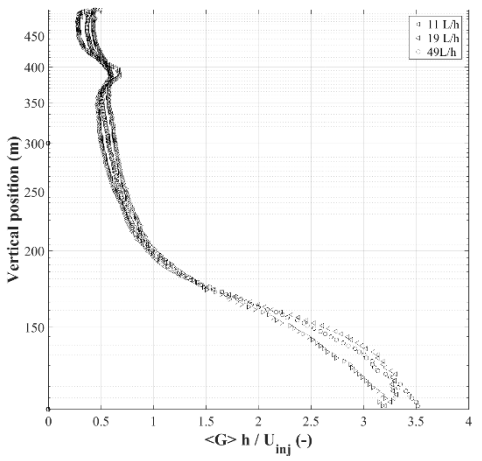

(c) horizontal averaged Kolmogorov scale	(d) normalised total velocity gradients

Figure 7. Vertical profiles of (a) mean velocity components along jet axis (X = 0 mm), (b) viscous dissipation rates of mean and turbulent kinetic energy, (c) and (d) mean flow and total turbulent gradients for the three flow rates (< 11 L/h, o 19 L/H, > 49 L/h)

After estimation of local viscous dissipation rate of turbulent kinetic energy, local velocity gradient G was estimated, based on local dissipation rate of total kinetic energy. These local values of viscous dissipation have been averaged in space along the width of the divergent; afterward, they have been averaged along Y (vertical average); thus, horizontal averaged of the velocity gradients were estimated (figure 7-d), and the global velocity gradients in the flocculation zone (Table 4). A first warning lies in the fact that the global value is defined as: $G(\langle\epsilon\rangle) = \sqrt{\frac{\langle\epsilon\rangle}{\nu}} \neq \langle G\rangle = \langle\sqrt{\frac{\epsilon}{\nu}}\rangle$.

The different results are given in Table 4. The flow rates, inlet velocities and residence times in the flocculation zone are recalled. Then the viscous dissipation rate of total kinetic energy is averaged in the plane of measurement in both horizontal and vertical directions. This is done in the two fields (figure 2), field 1 and field 2 and we observe that the viscous dissipation rate is 10 times higher close to the jet inlet where velocity gradient are stronger. The associated global velocity gradients are estimated and are $\sqrt{10}$ times greater in the bottom field and are proportional to the flowrate. Then, the velocity gradient averaged over the whole flocculation zone (once again in the vertical plane of PIV measurement) is calculated. $G(< \varepsilon_{Floc\_zone} >)$ ranges between 3 and 13 s^{-1}, whereas the global values estimated initially (Table 1) were in the range 2-14 s^{-1}. If we multiply these velocity gradients averaged over the whole flocculation zone by the residence time in the flocculation zone $G(< \varepsilon_c >) \times t_{RE}$, we obtain an almost constant value close to 7000 for the three flow rates.

Table 4 Estimation of global velocity gradients in flocculation zone, based on PIV data processing

Q (L/h)	Injected flow rate	11	19	49
U (m/s)	Injection velocity	0.24	0.42	1.08
t_{RF} (h)	Residence time in flocculation zone	0.636	0.368	0.143
$< \varepsilon_{Field\_1} >$ (m^2/s^3)	Average ε in field 1 zone	$1.8\ 10^{-6}$	$4.0\ 10^{-6}$	$3.6\ 10^{-5}$
$G(< \varepsilon_{Field\_1} >)$ (s^{-1})	Velocity gradient in field 1 zone	1.34	2.	6
$< \varepsilon_{Field\_2} >$ (m^2/s^3)	Average ε in field 2 zone	$1.7\ 10^{-5}$	$5\ 10^{-5}$	$3\ 10^{-4}$
$G(< \varepsilon_{Field\_2} >)$ (s^{-1})	Velocity gradient in field 2 zone	4.1	7.1	17.2
$< \varepsilon_{Floc\_zone} >$ (m^2/s^3)	Average ε in flocculation zone	$9.3\ 10^{-6}$	$2.7\ 10^{-5}$	$1.7\ 10^{-4}$
$G(< \varepsilon_{Floc\_zone} >)$ (s^{-1})	Velocity gradient in flocculation zone	3.06	5.2	12.9
$G(< \varepsilon_c >) \times t_{RE}$ (-)	First non-dimensional velocity gradient	7010	6890	6640
$G(< \varepsilon_c >) / (U / h)$	Second non-dimensional velocity gradient	1.28	1.24	1.19

As shown in the last lines of table 4, two non-dimensional velocity gradients are defined: (1) global G (square root of space average dissipation divided by the viscosity) times flocculation zone residence time or (2) global G (square root of space average dissipation divided by the viscosity) times (depth/U injection); whatever the definition, the non-dimensional global velocity gradient give constant values for the different flow rates. Since the velocity gradients in the flocculation zone evolve always more or less linearly with the inlet flow, as the residence time is inversely proportional to the flow rate, the Camp and Stein criteria *Gt* parameter recommended to achieve efficient flocculation will be almost constant.

Table 5 Values of velocity gradients in the whole jet clarifier

Q (L/h) Injected flow rate	11	19	49
$\langle G \rangle$ (s^{-1})	2.1	4.7	14.3

<G> PIV planes (s^{-1})	2.18	3.74	9.4
Residence time t_{res} (h)	3.82	2.21	0.86
$\langle G \rangle$ global x t_{res}	28,500	37,500	44,150
<G> PIV plane x t_{res}	29,980	29,760	29,100

Finally, the results on velocity gradients are summarized in Table 5 for the whole jet clarifier. Initially, global estimations of velocity gradients were obtained from global analysis where the total dissipation rate is calculated from a balance with the supplied power at the injection. In table 5, they are compared to the PIV measured velocity gradients, averaged over the 4 PIV planes and derived from local estimation of the shear rate (in terms of local viscous dissipation rate of kinetic energy, given by the sum of equations 16 and 17). On the whole jet tank again, the global velocity gradient increases linearly with the jet flow rate whereas the residence time decreases linearly. Consequently, the product *G t* remains constant close to 30000 for the 4 PIV fields whereas it was close to 7000 for first two fields near in the flocculation zone. In the same time, the residence time in increased 6 times (the ratio of the total volume divided buy the flocculation volume), it means that the average velocity gradient decreases rapidly around 60% between the two first fields and the two following (comparison between table 4 and 5).

This is a very interesting result that will be exploited to explain the efficiency of such a jet clarifier in terms of flocculation. Recall that during the residence time in the flocculation zone, there is a loop of circulation with a circulation time 10 times smaller than the flocculation residence time. The flocculation zone is thus a mixing zone very efficient to perform floc aggregation, followed by a clarification zone where the velocity gradient decrease progressively and the residence time increase linearly with the velocity reduction due to the geometrical enlargement.

Conclusion

In order to understand the good efficiency of a jet clarifier, a hydrodynamic study was led. In order to use PIV technique for local analysis, a quasi-bidimensional pilot was designed. Three flow rates were investigated which correspond to residence time from 1h to 4h. The local hydrodynamic analysis was limited to the flocculation zone (fields 1 & 2 of figure 2) near the jet inlet where the global velocity gradient *G* is higher. Results concerning the hydrodynamics of the flocculation zone reveal that the velocity fields exhibit a large circulation loop (figure 4). Circulation flow rates are estimated as well as circulation time that are 10 times larger at least than the residence time in this zone. The characteristic shape of the jet is also investigated, in terms of vertical distribution of its width. Then the outflow is analysed, and the outward flow rate is shown to be close to the inlet flow rate. These features are similar for the three flow rates. Vertical distributions of both the jet width and the vertical velocity divided by the inlet velocity are superimposed, confirming that the velocity field in the flocculation zone only depends on the inlet velocity. The flow structures (circulation) are similar and the amplitude of the velocities are proportional to the inlet (jet) velocity. During the residence time in the flocculator zone, there is a loop of circulation with a circulation time 10 times smaller than the residence time. The flocculation zone is thus a mixing zone very efficient to perform floc aggregation.

In the discussion, both local and global (time and space averaged) velocity gradients were addressed. First local viscous dissipation rates of turbulent kinetic energy were derived from PIV data; thus, the local velocity gradients, G, were estimated. Then, these local values of dissipation rate have been averaged in space along the width of the divergent; afterward, they have been averaged along Y (vertical average); thus, the horizontal average of velocity gradients G (horizontal average, figure 7-d) and their global average were estimated (Table 4)., in order to get global velocity gradients. The vertical profiles of horizontal average velocity gradients normalised by the inlet velocity are superimposed. Finally, the velocity gradients averaged over the whole flocculation zone were calculated. They range between 3 and 13 s^{-1} (Table 4), whereas the global values estimated initially (Table 1) were in the range 2-14 s^{-1}. Increasing the inlet jet flow rate, the global velocity gradients increase linearly with the jet flow rate whereas the residence time decreases linearly. Consequently, the global product *G t* remains

constant in this region where 10 loops are followed during the flocculation process; such circulation may contribute to the strength of the flocs. This is a very interesting result that will be exploited to explain the efficiency of such a jet clarifier in terms of flocculation.

Acknowledgements

This work was supported by Royal Golden Jubilee Ph.D. Program (Grant No. PHD/0152/2558) under Thailand Research Fund (TRF) and French Embassy in Thailand. Funding last year of Ploypailin Romphophak PhD was supported by the team Transfer-Interface-Mixing from Toulouse Biotechnology Institute in Toulouse.

References

Bickley, W. 1937. The plane jet. London Edinburgh Dublin Philos. Mag. J. Sci., 23(7), 727–731. doi: https://doi.org/10.1080/14786443708561847

Camp, T. R., & Stein, P. C. (1943). Velocity Gradients and Internal Work in Fluid Motion. Journal of Boston Society of Civil Engineering, 30, 219-237

Cleasby, J. L. 1984. Is Velocity Gradient a Valid Turbulent Flocculation Parameter, Journal of Environmental Engineering. 110(5), 875-897. doi: https://doi.org/10.1061/(ASCE)0733-9372(1984)110:5(875)

Clark, M. M. 1985. Critique of camp and Stein's RMS velocity gradient. Journal of Environmental Engineering (United States), 111(6), 741-754. doi: https://doi.org/10.1061/(ASCE)0733-9372(1985)111:6(741)

Degremont, S. A. 2007. Water treatment handbook , Lavoisier Publishing.

Delafosse A., Collignon M.-L., Crine M., and Toye D. 2011. Estimation of the turbulent kinetic energy dissipation rate from 2D-piv measurements in a vessel stirred by an axial Mixel TTP impeller. Chemical Engineering Science 66(8), 1728–1737. doi: https://doi.org/10.1016/j.ces.2011.01.011

Fossett, H., & Prosser, L. E. 1949. The Application of Free Jets to the Mixing of Fluids in Bulk. Proceedings of the Institution of Mechanical Engineers, 160(1), 224–232. doi: https://doi.org/10.1243/PIME_PROC_1949_160_024_02

Fossett, H. 1951. The action of free jets in mixing of fluids, Trans. Inst. Chem. Eng. 29, 322–332

Fox, E.A. and Gex, V.E. 1956, Single-phase blending of liquids. AIChE Journal., 2(4), 539-544. doi: https://doi.org/10.1002/aic.690020422

Garland, C., Weber-Shirk, M., and Lion, L. W. 2017. Revisiting Hydraulic Flocculator Design for Use in Water Treatment Systems with Fluidized Floc Beds. Environmental Engineering Science, 34(2), 122-129. doi:https://doi.org/10.1089/ees.2016.0174

Grenville, R. K. and Tilton, J. N. 1996. A New Theory Improves the Correlation of Blend Time Data from Turbulent Jet Mixed Vessels. Chem. Eng. Res. Des. 74, 390-396.

Grenville, R.K. and Tilton, J. N. 1997. Turbulence of flow as a predictor of blend time in turbulent jet mixed vessels. Proceedings of 9th European Conference on Mixing, 67-74.

Grenville, R. K. and Tilton, J. N. 2011. Jet mixing in tall tanks: Comparison of methods for predicting blend times. Chemical Engineering Research and Design, 89, 2501-2506.

Hiby, J.W., Modigell, M. 1978. Experiments on jet agitation, 6th CHISA congress, Prague

Jayanti S. 2001. Hydrodynamics of jet mixing in vessels, Chemical Engineering Science, 56(1), 193-210. doi: https://doi.org/10.1016/S0009-2509(99)00588-6

Kennedy, S., Bhattacharjee, K. P., Bhattacharya, N. S., Eshtiaghi, N., and Parthasarathy, R. 2018. Control of the mixing time in vessels agitated by submerged recirculating jets. Royal Society Open Science 5(1):171037. doi: https://doi.org/10.1098/rsos.171037

Kramer, T. A., and Clark, M. M. 1997. Influence of strain-rate on coagulation kinetics. Journal of Environmental Engineering, 123(5), 444–452. doi: https://doi.org/10.1061/(ASCE)0733-9372(1997)123:5(444)

Lee, J.H.W. and Chu, V.H. 1996. General integral formulation of turbulent buoyant jets in cross-flow. Journal of Hydraulic Engineering. 122(1). doi: https://doi.org/10.1061/(ASCE)0733-9429(1996)122:1(27)

Lee, H., and Hwang, W. 2019. Error quantification of 3D homogeneous and isotropic turbulence measurements using 2D PIV. International Journal of Heat and Fluid Flow, 78, 108431. doi:https://doi.org/10.1016/j.ijheatfluidflow.2019.108431

Marques, R. D. O., and Ferreira, S. S. F. 2017. Flocculation kinetics of low-turbidity raw water and the irreversible floc breakup process. Environmental Technology, 38(7), 901-910. doi:10.1080/09593330.2016.1236149

Maruyama, T., Kamishima, N., and Mizushina, T. 1984. An investigation of bubble plume mixing by comparison with liquid jet mixing. Journal of Chemical Engineering of Japan, 17(2), 120-126, doi: https://doi.org/10.1252/jcej.17.120

Maruyama, T., Ban, Y., and Mizushina, T. 1982. Jet mixing of fluids in tanks. Journal of Chemical Engineering of Japan, 15(5), 342–348. doi: https://doi.org/10.1252/jcej.15.342

Miller, D. R. and Comings, E. W. 1957. Static pressure distribution in a free turbulent jet. Journal of Fluid Mechanics 3, 1 –16. doi: https://doi.org/10.1021/ie50570a029

Mollendorf, J., & Gebhart, B. 1973. An experimental and numerical study of the viscous stability of a round laminar vertical jet with and without thermal buoyancy for symmetric and asymmetric disturbances. Journal of Fluid Mechanics, 61(2), 367-399. doi:10.1017/S0022112073000765

Pani, B. S., and Patil, L. G. 2007. Single-basin jet flocculators. Journal of Hydro-environment Research, 1(1), 20-29. doi:10.1016/j.jher.2007.04.002

Pearce, A.F., "Critical Reynolds Number for Fully-Developed Turbulence in Circular Submerged Water Jets", Council for Scientific and Industrial Research, Report MEG 475, Pretoria, South Africa, August 1966

Pedocchi, F. and Piedra-Cueva, I. 2005. Camp and Stein's Velocity Gradient Formalization. Journal of Environmental Engineering, 131, 1369-1376. doi: https://doi.org/10.1061/(ASCE)0733-9372(2005)131:10(1369)

Perumal, R., and Saravanan, K. 2012. Experimental Investigation on Mixing time Analysis of Jet Mixer

Res. J. Engineering Sci., 1(5), 7-11.

Randive, P. S., Singh, D. P., Varghese, V., and Badar, A. M. 2018. Study Of Jet Mixing In Flocculation Process - IJIRMPS 6(4), 76-85. DOI 10.17605/OSF.IO/2GJM8

Romphophak, P., Wongwailikhit, K., Chawaloesphonsiya, N., Samornkraisorakit, P., and Painmanakul, P. 2016. Study of Flow Pattern in Jet Clarifier for Removal of Turbidity by Residence Time Distribution Approach. Engineering Journal, 20(2), 17-27. doi:10.4186/ej.2016.20.2.17

Scharnowski, S., Grayson, K., de Silva, C. M., Hutchins, N., Marusic, I., and Kähler, C. J. 2017. Generalization of the PIV loss-of-correlation formula introduced by Keane and Adrian. Experiments in Fluids, 58(10), 150. doi:10.1007/s00348-017-2431-x

Schlichting, H. Boundary Layer Theory, 7th ed. McGraw-Hill, New York (1979)

Sobrino, J.A.H., Thiem, L.T., Alkhatib, E., 1996. Optimizing submerged jet flocculator performance. Journal American Water Works Association, 88, 81 – 92. doi:https://10.1002/J.1551-8833.1996.TB06602.X

M.R. von Smolan Smoluchowski, Drei Vorträge über Diffusion,Brownsche MolekularBewegung und Koagulation von Kolloidteilchen, Physikaliche Zeitschrift, Jg.17, p. 557-571, 585-599 (1916)

Wasewar, K. L., 2006. A Design of Jet Mixed Tank. Chem. Biochem. Eng. Q., 20(1), 31 – 46.

Nomenclature

C_2, C_3	(-)	constant
d	(m)	nozzle diameter
G	(s^{-1})	velocity gradient
h	(m)	depth of the pilot
J_0	(kg m s^{-2})	flux of momentum
m	(kg)	mass
P	(W)	supplied power
Q	(m^3 s^{-1})	injected flow rate
Q_C	(m^3 s^{-1})	circulation flow rate
r	(m)	radial position
R	(m)	nozzle radius
Re	(-)	Reynolds number
S	(s^{-1})	symmetric part of the velocity gradient tensor

S_{CS}	(m^2)	nozzle cross-section
t	(s)	contact time
t_C	(s)	circulation time
t_{RE}	(s)	residence time in flocculation zone
U	($m\ s^{-1}$)	axial or vertical velocity
U_{MAX}	($m\ s^{-1}$)	maximum axial or vertical velocity
u’	($m\ s^{-1}$)	axial or vertical turbulent velocity
Vol	(m^3)	volume
V	($m\ s^{-1}$)	radial or horizontal velocity
v’	($m\ s^{-1}$)	axial or vertical turbulent velocity
W	($m\ s^{-1}$)	velocity component
w’	($m\ s^{-1}$)	turbulent velocity component
X	(m)	horizontal coordinate
Y	(m)	vertical coordinate
ε	($m^2\ s^{-3}$or W/kg)	viscous dissipation of kinetic energy
η	(m)	Kolmogorov scale
$\dot{\gamma}$	(s^{-1})	shear rate
ν	($m^2\ s^{-1}$)	kinematic viscosity
ρ	($kg\ s^{-3}$)	density

θ	(rad)	angular coordinate

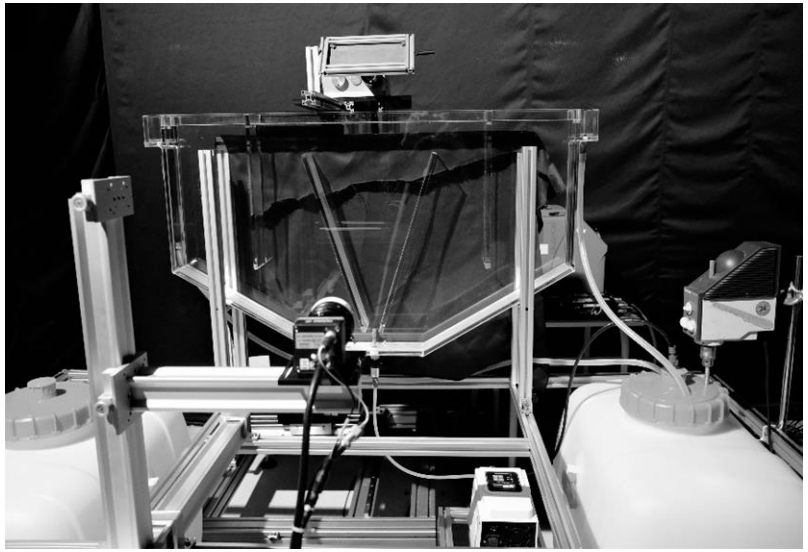

Quasi-2D Jet Clarifier

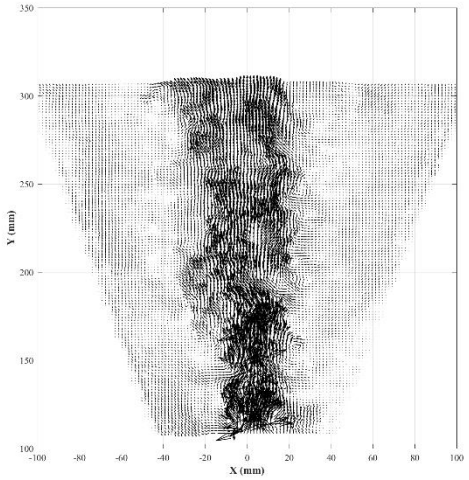

Instantaneous velocity field

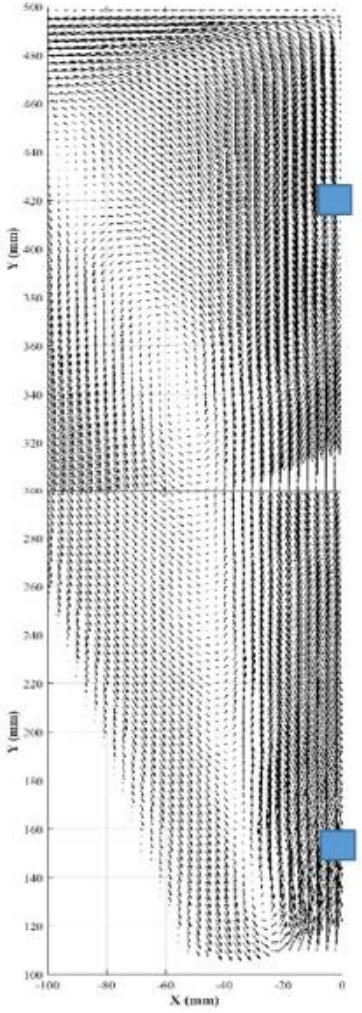

Mean velocity field:
circulation loop

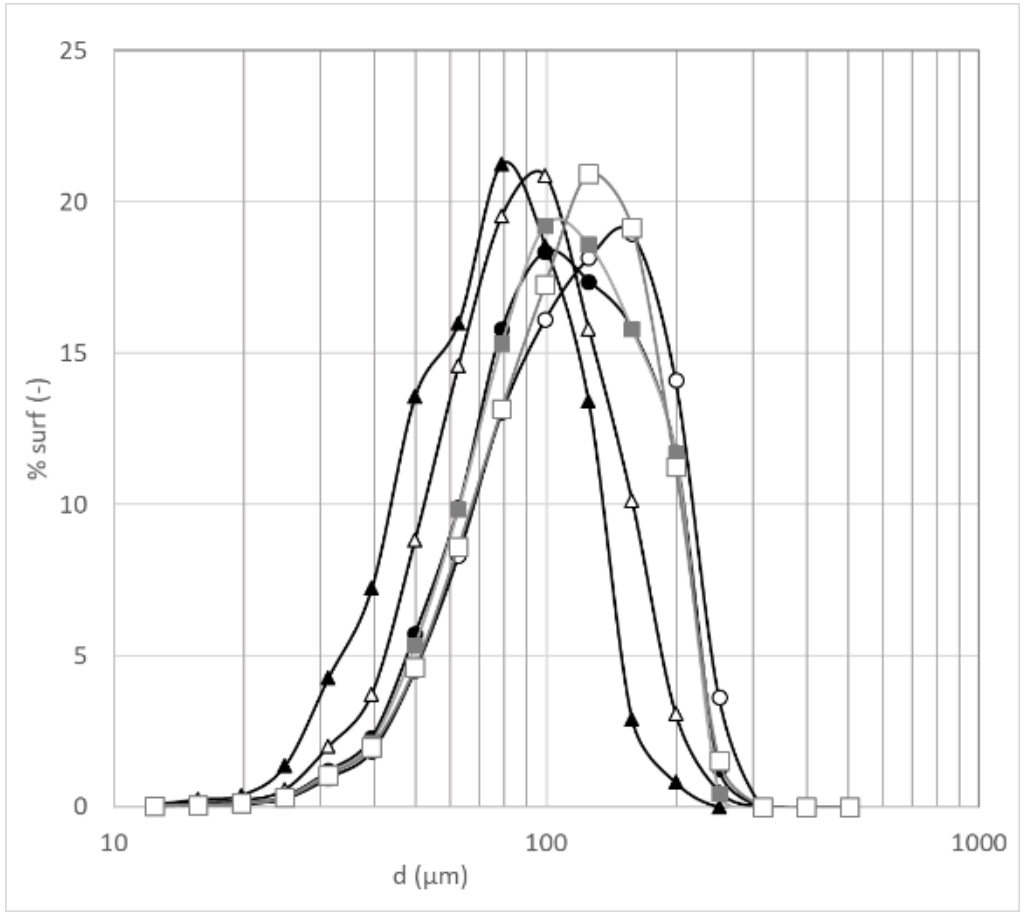

Steady-state floc size distributions
for 2 positions and 3 flow rates